XVIII IMEKO WORLD CONGRESS
Metrology for a Sustainable Development
September, 17 – 22, 2006, Rio de Janeiro, Brazil

A FEM ANALYSIS OF A NEGATIVE FREE DEFORMATION PRESSURE BALANCE OPERATING UP TO 100 MPa

G. Buonanno [1], *G. Giovinco* [1], *G. Molinar Min Beciet* [2], *P. Delajoud* [3], *R. Haines* [3]

[1] DiMSAT, University of Cassino, Cassino, Italy, buonanno@unicas.it [a]
[2] Istituto Nazionale di Ricerca Metrologica (I.N.RI.M.), Torino, Italy, g.molinar@inrim.it
[3] DH Instruments, Phoenix, AZ, USA, rhaines@dhinstruments.com

Abstract: The main purpose of this work is the numerical and experimental analysis of an innovative negative free deformation pressure balance. The numerical prediction of the pressure distortion coefficient, the piston fall rates, the piston-cylinder elastic distortions is achieved through the Finite Element Method (FEM). The numerical results are compared to the experimental values.

Keywords: pressure balance, Finite Element Method, pressure distortion coefficient.

1. INTRODUCTION

On the basis of a consolidated bilateral cooperation between INRIM/University of Cassino and DH Instruments [1], it was decided to test how finite element calculation methods can be a useful tool to predict the performance of an innovative negative free deformation pressure balance.

The pressure balance under investigation is the DHI-PG7202 type operating in negative free deformation mode up to 100 MPa [2].

PG7202 provides very high pressure gas operation using a unique gas operated, liquid lubricated piston-cylinder system. The principle of operation is shown in Figure 1. The measured gas pressure, P_m, is applied to the bottom of the piston and to the top of a liquid reservoir located around the cylinder. The liquid used in this analysis is di-hethyl-hexyl sebacate. The reservoir is connected to the gap between the piston and the cylinder through lateral holes near the bottom of the cylinder, allowing liquid from the reservoir to enter the gap. The pressure of the liquid in the lubricating holes, P_l, is equal to the gas pressure P_m, plus the pressure due to the liquid head, h. Therefore, the liquid pressure in the gap is always higher than the gas pressure by the amount of the liquid head regardless of the gas pressure value. Since h is small and the space between the piston and cylinder is typically less than 1 micrometer, the bleed of liquid from the bottom of the cylinder towards the gas pressure is extremely small. The principle upward flow of liquid lubricates the active zone of the piston-cylinder as in a typical oil piston-cylinder.

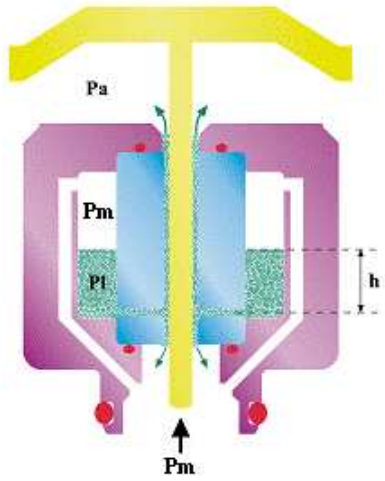

Fig. 1 – PG7202 Gas operated, liquid lubricated piston-cylinder operating principle

2. BASELINE MODEL

The simplified geometry of the model is shown in Fig. 2 whereas the corresponding coordinates of the main points are shown in Tab. I.

The mechanical theory of elastic equilibrium allows determination of the elastic distortion of the piston and cylinder, with a known pressure distribution acting along the clearance. Such distortions are obtained using the elastic equilibrium conditions on the piston-cylinder. In the hypothesis of axial symmetric loads and geometry, the system of equations in cylindrical co-ordinates (z, r, θ) is reported in [3].

The solution of the system of equations can be numerically obtained through the Finite Element Method (FEM) in order to evaluate the effective piston-cylinder clearance on the basis of the following relationship:

$$h(z) = h_0 + U(z) - u(z) \quad (1)$$

where h_0, U and u are the undistorted radial clearance, the cylinder radial displacement and the piston radial displacement, respectively.

[a] (Author for contacts)

Tab. I – Coordinates of the main cylinder and piston points

Point	*r* coordinate mm	z coordinate mm
C_1	1.2496	0
C_2	1.2496	20.76
C_3	1.2496	23.5
C_4	4.825	23.5
C_5	7.75	23.5
C_6	9.5	23.5
C_7	10.0	23.0
C_8	10.0	-6.0
C_9	9.5	-6.5
C_{10}	1.2496	-6.5
C_{11}	1.2496	-3.0
C_{12}	1.75	-2.0
C_{13}	1.75	-1.0
P_1	0	-16.5
P_2	1.24885	-16.5
P_3	1.24885	0
P_4	1.24885	20.76
P_5	1.24885	23.5
P_6	1.24885	43.5
P_7	0	43.5

On the other hand, the distribution of pressure $p(z)$ along the clearance can be determined by means of the fluid-dynamic theory of laminar flow, the radial clearance dimension $h(z)$ being known from the previous calculation step through eq. (1). Assuming one-dimensional laminar flow, stationary regime, Newtonian fluid, and constant temperature, the clearance pressure distribution is given by the Navier-Stokes equations as [3, 4]:

$$p(z) - p_a = -\frac{6 \cdot \dot{m}}{\pi \cdot r\left(z = z_m\right)} \cdot \int_{z_m}^{z} \frac{\eta(p,t)}{\rho(p,t)} \frac{1}{h(z)^3} dz \qquad (2)$$

where p_a is the atmospheric pressure, z_m is the axial clearance coordinate where the measured pressure p_m is applied, $\dot{m}$ is the working fluid mass flow rate, $\eta(p,t)$ and $\rho(p,t)$ are the dynamic viscosity and the density of the working fluid respectively which are both pressure and temperature dependent. Once the functional link between the fluid thermo physical properties and pressure is known after different iterations between the distortions and the pressure distribution, the value to be assumed for the mass flow $\dot{m}$ is obtained by means of:

$$-\frac{6\dot{m}}{\pi \cdot r_p} = \frac{p_m - p_a}{\int_{z_a}^{z_m} \frac{\eta(p,t)}{\rho(p,t)} \frac{1}{h(z)^3} dz} \qquad (3)$$

The boundary conditions, in relation to the geometric domain given in Fig. 2 are:

Cylinder boundary conditions

1) $p(r,z) = p_{gap}$ for each (r,z) belonging to $\overline{C_1C_3}$
2) $p(r,z) = p_a$ for each (r,z) belonging to $\overline{C_3C_4}$
3) $p(r,z) = p_{cont}$ for each (r,z) belonging to $\overline{C_4C_5}$

The contact pressure profiles were determined by stress and deformation analysis of the contact between the cylinder top and upper cylinder sleeve through the 3D FEM software (Cosmos/M) and results are given in Fig. 3.

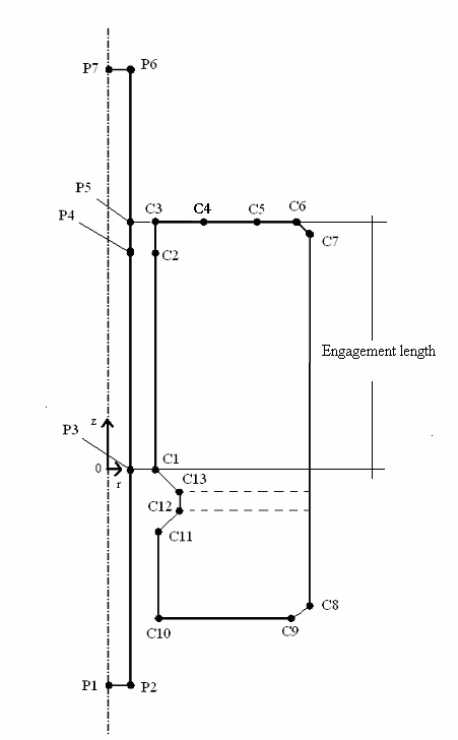

Fig. 2 – Simplified geometrical model adopted

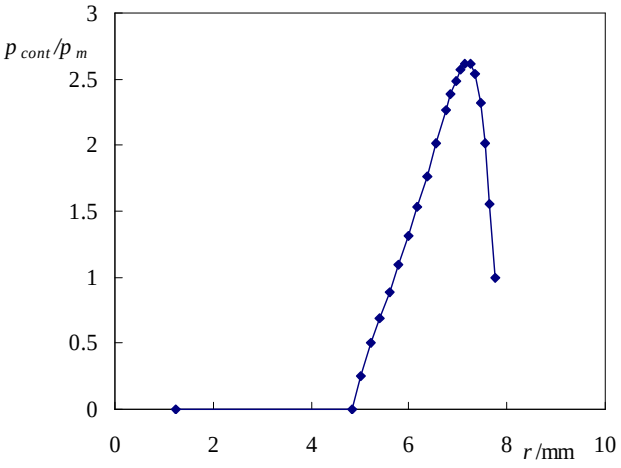

Fig. 3 – PG7202 dimensionless contact pressure

4) $p(r,z) = p_m$
for each (r,z) belonging to $\overline{C_5C_6C_7C_8C_9C_{10}C_{11}C_{12}C_{13}C_1}$
5) $w(r,z) = 0$ at C_5

Piston boundary conditions

1) $p(r,z) = p_m$
for each (r,z) belonging to $\overline{P_1P_2}$ and $\overline{P_2P_3}$

2) $p(r,z) = p_{gap}$

for each (r,z) belonging to $\overline{P_3P_4}$ and $\overline{P_4P_5}$

3) $p(r,z) = p_a$ for each (r,z) belonging to $\overline{P_5P_6}$

4) $u(r,z) = 0$ for each (r,z) belonging to $\overline{P_1P_7}$

5) $w(r,z) = 0$ for each (r,z) belonging to $\overline{P_6P_7}$

In order to obtain the clearance pressure distribution, eq. (2) has to be solved iteratively, since the radial gap and the fluid thermo physical properties depend on pressure.
Therefore, at the first iteration a linear pressure profile along the clearance is applied and, then, the corresponding elastic deformations of the piston-cylinder system and the new clearance profile *h(z)* are evaluated by means of the elastic equilibrium equations solved through the FEM. The obtained clearance profile is replaced in eq. (2) together with the thermo physical fluid properties evaluated with the present pressure distribution, leading to a new pressure distribution *p(z)* to be applied along the clearance at the next iteration. The measurement principle of pressure balances is based on the equilibrium of the forces acting on the piston in vertical direction. The forces acting upward are [3]:

$$F_b + F_f + F_p = \\ = \pi p_m r_0(0)^2 \left[1 + 2\frac{u(0)}{r_0(0)}\right] + 2\pi \int_{z_a}^{z_m} r(z)\left(-\frac{h(z)}{2}\frac{dp(z)}{dz}\right)dz + \\ + 2\pi \int_{z_a}^{z_m} r(z)\left(p(z)\frac{dr(z)}{dz}\right)dz = p_m A_e \quad (4)$$

where r is the deformed piston radius, F_b represents the force due to the applied pressure on the basis of the piston, F_f is the shear stresses of the fluid acting on the lateral surface of the piston and F_p is the force due to the vertical component of the pressure applied to the lateral surface of the piston. From eq. (4) it can be deduced that the knowledge of the effective area A_e, by knowing the force acting downward the piston, is necessary to evaluate the measured pressure, p_m. On the other hand, from the elastic distortion theory it can be demonstrated that, on the hypothesis of linear variation of the effective area A_e of a negative free deformation piston-cylinder unit with applied pressure, the following functional relationship can be adopted:

$$A_e = A_0 \cdot (1 + \lambda \cdot p_m) \quad (5)$$

where A_0 is the effective area at zero pressure, the deviations from linearity being small in practice.

The evaluation of the pressure distortion coefficient using eq. (4) at each iterative step can be made once the interrelated quantities *u(z)*, *U(z)* and *p(z)* are known. The convergence of the iterative procedure is reached if $\frac{A_{e,i} - A_{e,i-1}}{A_{e,i}} < 10^{-6}$, where i is the iteration step index. The convergence can be evaluated as well on the pressure values in each point of the clearance along the engagement length until the pressure value in the clearance is constant within $1 \cdot 10^{-8}$ of the pressure value.

3. NUMERICAL RESULTS FOR THE BASELINE ANALYSIS

The FEM numerical results for the baseline model and for the different measured pressure p_m values from 6 to 100 MPa can be summarised in the following way.

Fig. 4 gives the normalised pressure distribution p^* in the clearance versus the normalised axial coordinate z^* in the piston-cylinder engagement length. The dimensionless coordinate z^* refers to the axial engagement length of the piston-cylinder engagement length ($z^* = 0$ for $z = z_m = 0.0$ mm which is the initial piston-cylinder engagement length and $z^* = 1$ for $z = z_a = 23.5$ mm which is the final piston-cylinder engagement length). Fig. 5 gives the values of the radial clearance gap h / μm versus the normalised axial coordinate z^*.

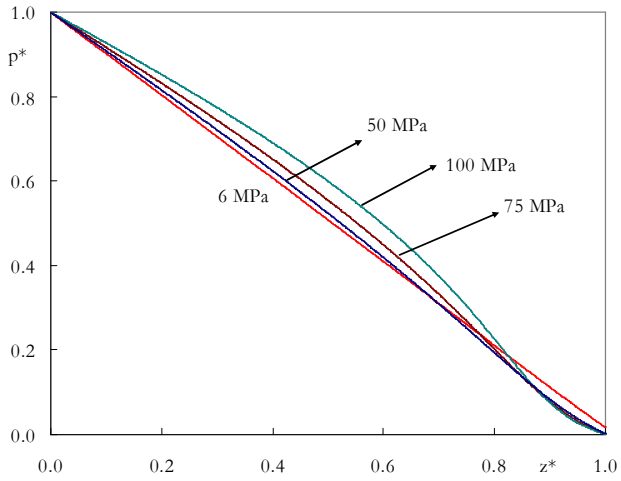

Fig. 4 - Normalized pressure distribution p^* in the clearance, at different measured pressures, versus the normalized piston-cylinder engagement length z^*

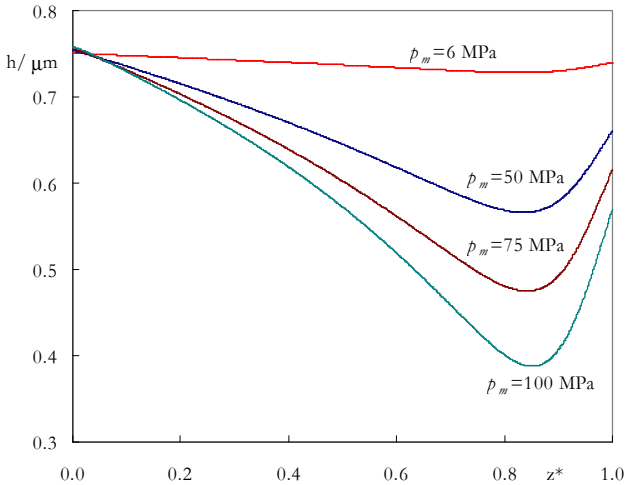

Fig. 5 – Radial clearance gap h at different measured pressures versus the normalized piston-cylinder engagement length z^*

From the above-mentioned figures, it can be noted that:

- the trend of the dimensionless pressure p^* in the clearance depends on the measured pressure and it shows, as usual, a non linearity that increases with the measured pressure p_m.
- the radial clearance gap, with exception of the beginning of the clearance, is always less than the undistorted value of 0.75 μm. The minimum radial clearance gap at 100 MPa is ≈ 0.39 μm at z^*=0.85.

In Fig. 6 the effective area vs. the measured pressure is reported.

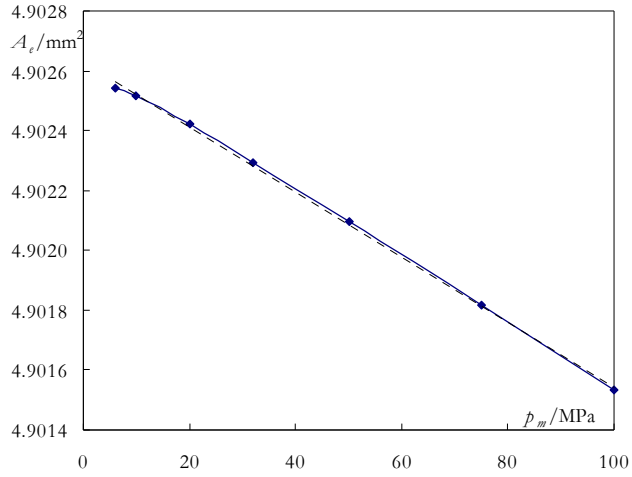

Fig. 6 – Effective area trend with respect to measured pressure

As can be seen from Fig. 6, the effective area determined by the numerical procedure (blue points) diminishes as the measured pressure increases in a nearly linear way. By extrapolating the linear trend (dashed line), the effective area at reference condition using FEM, $A_{0,num}$ is determined (equal to 4.902628 mm^2) and compared to the theoretical value, $A_{0,theor}$, (obtained as mean value between the piston and the cylinder area and equal to 4.902654 mm^2). A difference of only 5.3 ppm is determined, confirming the validity of the numerical procedure.

Taking in to account of the practical use of the pressure balance, with reference exclusively to the λ value, we consider a good choice a value of λ = -2.21·10^{-6} MPa^{-1} in all the examined pressure range (obtained by means of a linear least squares regression). In this case, the maximum difference in the range 20-100 MPa between the proposed value and the numerical ones is 0.11 10^{-6} MPa^{-1}.

As regards the piston fall rate, Fig. 7 shows the values at 20 °C for the nominal clearance vs. the measured pressure. The piston fall rate presents a non monotonic trend as pressure increases and assumes a maximum value of 2.32 μm/s at 50 MPa (corresponding to the middle of the pressure balance range).

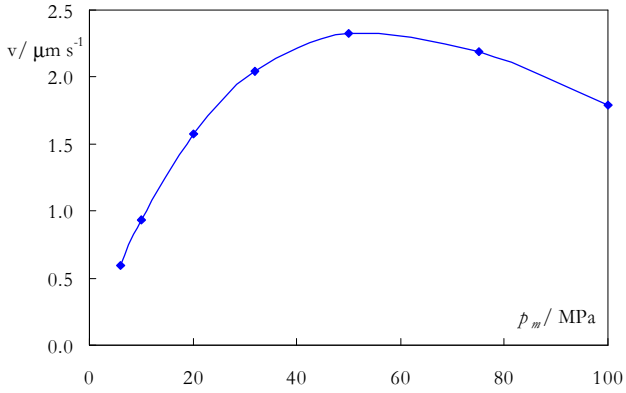

Fig. 7 – Piston fall rate at 20 °C for the nominal clearance vs. the measured pressure

3.1 Sensitivity analysis related to the pressure distortion coefficient and piston fall rate

The estimation of the pressure distortion coefficient using the FEM depends on, as previously shown, different parameters or physical quantities. The estimated standard uncertainties of the pressure distortion coefficient and of the piston fall rate resulting from FEM modelling calculations are evaluated by considering the standard uncertainties of the input quantities, $(\partial\lambda/\partial x_i)\cdot u(x_i)$, where $(\partial\lambda/\partial x_i)$ are the sensitivity coefficients of each parameter or physical quantity. Even if it is always possible to evaluate these sensitivity coefficients with good reliability (with exception of clearance shape and dimensional irregularities that need very careful dimensional measurements of both piston and cylinder), the complexity and the variability of the functional link (as the characteristics of the pressure balances can change from model to model also due to complex influence of specific boundary conditions) do not allow to obtain an unique equation for every kind of pressure balance. Therefore, the most suitable approach in the determination of the sensitivity coefficients seems to be the numerical approach based on the finite differences [5]. For each case of sensitivity, a full FEM numerical calculation of *u, U, h* and piston fall rate is made in order to determine the appropriate sensitivity coefficient related to the selected variable.

As regards the influence of the elastic properties of the piston-cylinder unit on the pressure distortion coefficient and on the piston fall rate, the corresponding sensitivity coefficients are reported in Tab. II, at p_m equal to 100 MPa. From Tab. II it can be noted that:

- an estimated uncertainty (used here as a variation) of ± 5 % on Young modulus E_p for the piston and on Young modulus E_c of the cylinder produces a contribution to the λ standard uncertainty equal to 1.4 10^{-8} MPa^{-1} and 1.0 10^{-7} MPa^{-1} that are equivalent to a $\Delta\lambda/\lambda$ of 0.6 % and of 4.4 % respectively, a relatively high uncertainty value in the case of the cylinder;
- similarly, as regards the Poisson ratio, a ± 5 % estimated uncertainty on Poisson ratio for the piston and the

cylinder determines a contribution to the λ standard uncertainty equal to 2.9 10^{-8} MPa^{-1} and 2.6 10^{-8} MPa^{-1} respectively, that are equivalent to a $\Delta\lambda/\lambda$ of 1.3 % and of 1.1 % respectively;

- the maximum value (6.7 %) for the piston fall rate corresponds to the Young modulus E_c of the cylinder.

Tab. II – Sensitivity coefficients of the pressure distortion coefficient and piston fall rate at 100 MPa

Quantity	**Standard uncertainty**	**Relative contribution to the standard uncertainty/ %**
x_i	$u(x_i)$	$\frac{\partial\lambda}{\partial x_i}\cdot\frac{u(x_i)}{\lambda}\cdot 100$
E_p=5.60 10^5 MPa	28 10^3 MPa	-0.6
E_c= 6.20 10^5 MPa	31 10^3 MPa	-4.4
μ_p= 0.218	1.1 10^{-2}	-1.3
μ_c = 0.218	1.1 10^{-2}	-1.1
x_i	$u(x_i)$	$\frac{\partial v}{\partial x_i}\cdot\frac{u(x_i)}{v}\cdot 100$
E_p=5.60 10^5 MPa	28 10^3 MPa	-1.2
E_c= 6.20 10^5 MPa	31 10^3 MPa	6.7
μ_p= 0.218	1.1 10^{-2}	-2.0
μ_c = 0.218	1.1 10^{-2}	1.8

The authors have developed an analysis for ± 0.2 μm constant variation of the nominal radial gap in the working region (C_1-C_3) to better understand the influence of the piston and cylinder undistorted gap on the pressure distortion coefficient and piston fall rates for different measured pressure p_m values from 6 to 100 MPa.

The distortion coefficient was found to be nearly constant, with a maximum variation of 2.3 10^{-8} MPa^{-1}, equivalent to a $\Delta\lambda/\lambda$ of 1%.

As expected the piston fall rate variations are very high (with a maximum value equal to 157.0 %) and the piston fall rate variations at lower pressures are less than the variations at higher pressures (Fig. 8).

The influence of the piston and cylinder undistorted gap can be also found in Fig. 9 where the normalized pressure distribution p^* in the clearance, at different undistorted gaps and at the measured pressure equal to 100 MPa, versus the normalized piston-cylinder engagement length z* are reported.

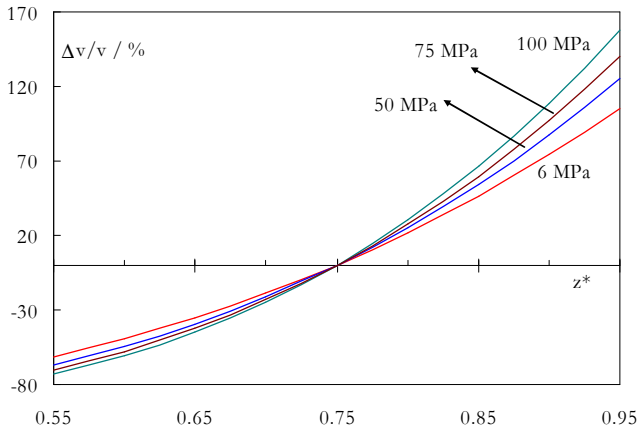

Fig. 8 – Piston fall rate differences in respect to baseline values at 20 °C vs. the radial clearance dimension as the different measured pressures p_m vary from 6 to 100 MPa

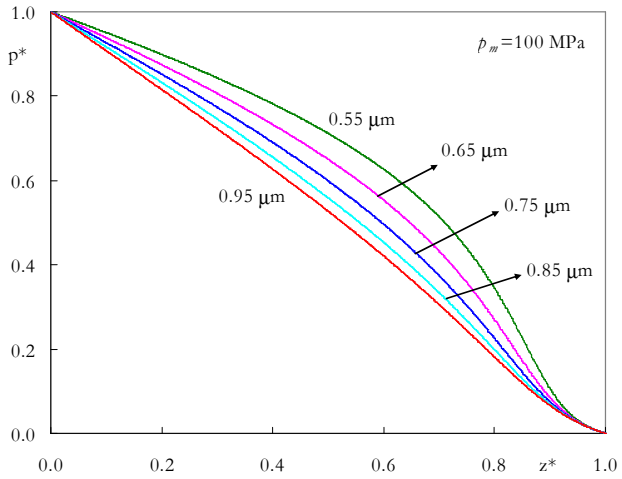

Fig. 9 – Normalized pressure distribution p^* in the clearance, at different undistorted gaps and at the measured pressure equal to 100 MPa, versus the normalized piston-cylinder engagement length z^*

From Fig. 9 the presence of high non linearity for smaller undistorted gaps can be noted, whereas the normalized pressure distribution presents a practically linear trend for an undistorted gap equal to 0.95 μm.

4. COMPARISON WITH EXPERIMENTAL RESULTS

All FEM calculated results are discussed and compared with the characteristics of production piston-cylinders available from the manufacturer of the pressure balances. The distortion coefficients were determined by cross float with well known oil reference standards. In Figure 10 they are compared with the numerical values. To show the magnitude of the deviation, limits representing ± 50 ppm of pressure at full scale are included. Also included is the theoretical calculation from the Klingenberg equation, which is gap independent. The FEM values show an interesting independence of the gap and align very well with the Klingenberg value which is a useful check of the

numerical procedure. It can be seen from the figure that there is very good agreement between the numerical and the experimental results as well as a clear convergence of the experimental results with the FEM numerical result with increasing gap.

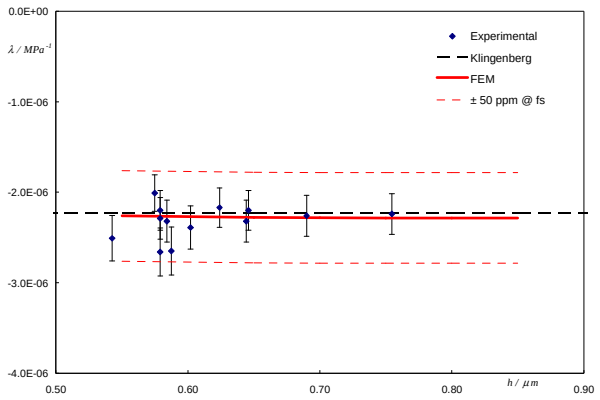

Fig. 10 – Experimental and Numerical Pressure Distortion Coefficient vs. Gap

The typical average undistorted gaps in the piston-cylinders under investigation are significantly smaller than the nominal gap used in the numerical calculation. In order to be able to compare the drop rate as a function of pressure the experimental results are normalized relative to the fall rate at 100 MPa. Figure 11 shows the experimental and numerical fall rates (normalized to the values listed in Tab. III).

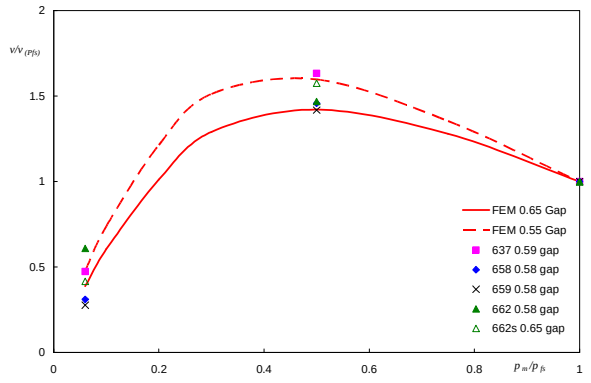

Fig. 11 – Experimental and Numerical Normalized Fall Rate vs. Normalized Pressure

Since the shape of the normalized fall rate is a function of undistorted gap, numerical values representing the envelope of the experimental gap values are shown.

The behavior of a negative free deformation system is not monotonic, as can be seen from the numerical study, with a maximum value near 50% of maximum pressure. The experimental values follow this trend very well, inside the gap envelope at mid pressure and with uniform and nearly symmetrical dispersion at low pressure where the uncertainty of fall rate determination is larger.

Tab. III – Experimental and Numerical Undistorted Mean Gaps and Fall Rates at 100 MPa

PC	$\bar{h}_0$ / μm	v_{exp} / μm.s^{-1}	v_{num} / μm.s^{-1}
637	0.588	0.42	0.65
658	0.575	0.47	0.59
659	0.579	0.40	0.61
662	0.579	0.36	0.61
662s	0.646	0.69	0.96
FEM	0.550		0.48
FEM	0.650		0.99

5 CONCLUSIONS

This is the first time that an iterative numerical method, taking into account both the mechanics and the fluid dynamics models, has been used to model and predict metrological characteristics of a negative free deformation piston-cylinder. The good agreement between the experimental and numerical data confirms the possibility of using this tool for prediction of performance of complex pressure balances.

The sensitivity analysis shows the importance of the value of the undistorted gap, both for the pressure distribution and for the piston fall rate. This numerical method is helpful for defining the optimum undistorted gap, a compromise between having the best linearity of the pressure distribution with improved prediction of the distortion coefficient, and having an acceptable piston fall rate.

REFERENCES

[1] G. Molinar, G. Buonanno, G. Giovinco, P. Delajoud, R. Haines, Effectiveness of finite element calculation methods (FEM) on highly precise and sensitive pressure balances in liquid media up to 200 MPa, **Metrologia,** 42, 207–211, 2005

[2] P. Delajoud and M. Girard, A new piston gauge to improve the definition of high gas pressure and to facilitate the gas to oil transition in a pressure calibration chain, **IMEKO TC16, International Symposium on pressure and vacuum, 2003 Sept. 22-24**, Beijing, China, Editor: Acta Metrologica Sinica Press, September 2003, 154-159

[3] Buonanno, M. Dell'Isola, G. Iagulli, G.F. Molinar, A finite element method to evaluate the pressure distortion coefficient in pressure balances, **High Temperatures High Pressures**, 31, pp 131-143, 1999

[4] Molinar G.F., Maghenzani R., Cresto P.C., Bianchi L., Elastic distortions in piston-cylinder units at pressures up to 0.5 GPa, **Metrologia**, 29, pp. 425-440, 1992.

[5] ISO, Guide to the Expression of Uncertainty in Measurement, Geneve, 1993

[6] W. Sabuga, G. Molinar, G. Buonanno, T. Esward, T. Rabault, and L. Yagmur, Calculation of the distortion coefficient and associated uncertainty of PTB and LNE 1 GPa pressure balances using finite element analysis - EUROMET Project 463, **Metrologia,** 42, 202–206, 2005